

Phase shift of cyclotron orbits at type-I and type-II multi-Weyl nodes

M. Breitzkreuz,^{1,2} N. Bovenzi,¹ and J. Tworzydło³

¹*Instituut-Lorentz, Universiteit Leiden, P.O. Box 9506, 2300 RA Leiden, The Netherlands*

²*Dahlem Center for Complex Quantum Systems and Fachbereich Physik, Freie Universität Berlin, 14195 Berlin, Germany*

³*Institute of Theoretical Physics, Faculty of Physics, University of Warsaw, ul. Pasteura 5, 02-093 Warszawa, Poland*

(Dated: March 2018)

Quantum oscillations of response functions in high magnetic fields tend to reveal some of the most interesting properties of crystals. In particular, the oscillation phase shift is sensitive to topological band features, thereby helping to identify the presence of Weyl fermions. In this work, we calculate the phase shift for Weyl fermions of type I and type II, predicting characteristic dependence of the phase shift on the topological charge of the quasiparticle. Surprisingly, the phase shift acquired by a particle that tunnels between the bands via magnetic breakthrough near a type-II Weyl point measures the topological charge most robustly—here the value does not depend on specifics of the band structure, in contrast to the most cases without tunneling.

Introduction—Electrons moving along cyclotron orbits in a homogeneous magnetic field are subject to the quantization condition [1]

$$l^2 S = 2\pi(m + \gamma), \quad m \in \mathbb{Z}, \quad (1)$$

where S is the zero-field area enclosed by the cyclotron orbit in momentum space, $l = \sqrt{\hbar/eB}$ is the magnetic length, and the offset γ includes quantum corrections, which can be expanded in powers of the magnetic field B [2]. In the semiclassical regime when the magnetic length is much larger than the Fermi wavelength, field-dependent corrections to γ are suppressed and the remaining number of zeroth order in B encodes valuable information about the electronic properties of the system. In particular, the offset includes contributions coming from topological features in the band structure [3–5], which makes it the subject of high current interest. Experimentally it can be deduced from quantum oscillations in the de Haas-van Alphen or the Shubnikov-de Haas effects, widely used nowadays to identify Weyl, Dirac, and nodal-line semimetals [6–10].

Interestingly, in some well-studied systems the offset measures the topological features independent of the specifics of the band structure. So, e.g., in graphene and graphene bilayer exposed to an out-of-plane magnetic field the offset turns out to be given by a winding number—the number of full circles made by a pseudo-spin degree of freedom of the particle (the nature of which is unimportant in this context) during a single circle around the cyclotron orbit [4]. This integer winding number is a robust feature, determined by the type of the band touching, and is sometimes called the topological charge of the Weyl or Dirac fermion [11]. In contrast to the common belief, however, the topological charge contributes to the offset in such a robust manner only in exceptional cases, namely when particular symmetry constraints are satisfied [5].

While the above considerations concern orbits that enclose a topological charge on a conventional (type-I) Weyl cone, much less is known about the offset of orbits that

measure the topological charge by passing the so-called type-II Weyl node [12]—a Weyl node with an overtilted cone as sketched in Fig. 1. Upon the type-I to type-II transition, the closed cyclotron orbit of a type-I Weyl semimetal is replaced by two open branches, which can be closed at large momenta by higher-order corrections to the Weyl Hamiltonian, resulting in two cyclotron orbits, one electron-like and one hole-like. Band details determine a critical magnetic field, above which the two separate cyclotron orbits effectively merge into a single orbit via magnetic breakthrough [13, 14]. This critical field is zero if the energy and the parallel momentum are exactly at the node where the two cyclotron orbits touch [15, 16], and is larger than zero if the gap between the two orbits is finite. The magnetic breakdown is an additional source for wavefunction phase jumps that contribute to the offset γ , so one would expect that the offset is generally even more sensitive to band details than in the case without breakdown.

In this work we analyze the offset of cyclotron orbits close to type-I and type-II Weyl points with an arbitrary topological charge n . For orbits at type-I Weyl points and

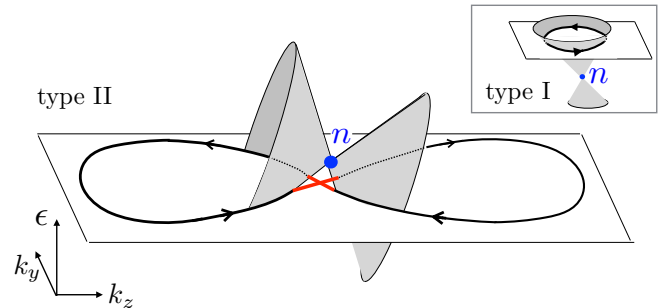


FIG. 1: Schematic illustration of a breakthrough cyclotron orbit (figure-8 curve) at a type-II Weyl node with topological charge n . The red part indicates quantum tunneling in the magnetic-breakthrough region. The inset shows a cyclotron orbit at a type-I Weyl node.

separated orbits at type-II Weyl points, we find characteristic dependence of γ on the topological charge and on band details. However, for the seemingly more complex breakthrough orbit at a type-II Weyl point, the offset turns out to depend only on the topological charge. This surprising result is based on two facts, the universality of the phase jump of π acquired in the magnetic-breakthrough region and a robust phase shift of $n\pi$ induced by the topological charge. The insensitivity of the latter on band details comes from a cancellation of a non-universal part of the phase in the two loops of the breakthrough orbit, which are traversed in opposite directions.

Model—We consider a set of Hamiltonians that govern the physics close to topologically distinct band touchings,

$$H_0 = k_- \sigma_+ + k_+ \sigma_- + u k_z \sigma_0, \quad (2a)$$

$$H_n = k_-^n \sigma_+ + k_+^n \sigma_- + u k_z \sigma_0 + k_z \sigma_z, \quad n \in \{1, 2, \dots\}, \quad (2b)$$

where $k_\pm = k_x \pm ik_y$, $\sigma_\pm = \sigma_x \pm i\sigma_y$, $\sigma_{x,y,z}$ are Pauli matrices, and σ_0 the identity matrix. The band touching described by H_i , $i \in \{0, 1, 2, \dots\}$, is the source of the topological charge located at $\mathbf{k} = 0$ with the value i . In particular, H_n corresponds to a topologically protected multi-Weyl node of order n [17], while H_0 describes a trivial, non-protected band touching. The parameter $u > 0$ controls the tilt of the Weyl cone; for $u < 1$ and $u > 1$ the Weyl cone is of type I and II, respectively.

The magnetic field pointing in the x direction moves the particles along cyclotron orbits $k_z(k_y)$ at a fixed energy ϵ and parallel momentum component k_x . The orbits are determined by the Schrödinger equation

$$H_n |u_{n\pm}\rangle = \epsilon |u_{n\pm}\rangle, \quad (3)$$

where \pm denote the two bands. In the quantization condition (1) one can distinguish three possible phase shifts that contribute to the offset

$$\gamma = \frac{1}{2\pi} (\phi_0 + \phi_b + \phi_t). \quad (4)$$

Here ϕ_0 and ϕ_b are phase shifts that occur at singular points on the orbit. Specifically, turning points give rise to the Maslov phase ϕ_0 [18], in which each turning point contributes a phase jump of $\pm\pi/2$, the sign determined by the sign of the curvature at the turning point. With ϕ_b we denote the phase shifts that occur due to magnetic breakdown. Finally, ϕ_t is the topological phase shift, which includes the Berry phase accumulated during a full turn around the orbit and the effect of the magnetic orbital moment [3–5, 19]. In the following we calculate the phases ϕ_b and ϕ_t separately.

Topological phase shift—The topological phase shift of a closed contour at energy ϵ and the fixed momentum component k_x is given by [4, 20]

$$\phi_t = \oint dk'_y \left[A - \frac{dk_z(k'_y)}{d\epsilon} M \right]. \quad (5)$$

Here the first term is determined by the Berry connection projected onto the contour,

$$A = i \langle u | \nabla_{\mathbf{k}} | u \rangle \cdot \frac{d\mathbf{k}}{dk_y} = i \langle u | \frac{d}{dk_y} | u \rangle, \quad (6)$$

which contributes to ϕ_t the usual Berry phase of the closed orbit. The second term is the correction to the zero-field area S coming from the magnetic orbital moment projected onto the direction of the magnetic field [19],

$$M = \frac{i}{2} \left[(\partial_{k_y} \langle u |) (\epsilon - H) (\partial_{k_z} | u \rangle) - (\partial_{k_z} \langle u |) (\epsilon - H) (\partial_{k_y} | u \rangle) \right]. \quad (7)$$

The eigenfunctions of the Hamiltonian H_i can be written as

$$\begin{aligned} |u_{0\pm}\rangle &= \frac{1}{\sqrt{2}} \begin{pmatrix} \mp e^{-i\alpha} \\ 1 \end{pmatrix}, \\ |u_{n+}\rangle &= \begin{pmatrix} -\sin \frac{\beta}{2} e^{-in\alpha} \\ \cos \frac{\beta}{2} \end{pmatrix}, \quad |u_{n-}\rangle = \begin{pmatrix} \cos \frac{\beta}{2} e^{-in\alpha} \\ \sin \frac{\beta}{2} \end{pmatrix}, \end{aligned} \quad (8)$$

where the angles α and β are defined as

$$\begin{aligned} \cos \beta &= \frac{k_z}{k}, \quad \sin \beta = \frac{(k_x^2 + k_y^2)^{\frac{n}{2}}}{k}, \\ \alpha &= \text{Arg}(k_x + ik_y), \quad k = \sqrt{(k_x^2 + k_y^2)^n + k_z^2}. \end{aligned} \quad (9)$$

In this gauge, we obtain from (6)–(9)

$$A_{0\pm} = \frac{k_x}{2(k_x^2 + k_y^2)}, \quad M_{0\pm} = 0, \quad (10)$$

$$A_{n\pm} = \frac{nk_x (k_x^2 + k_y^2)^{n-1}}{2k(k \pm k_z)}, \quad (11)$$

$$M_{n\pm} = -\frac{nk_x (k_x^2 + k_y^2)^{n-1}}{2k^2}. \quad (12)$$

For topologically trivial H_0 we immediately see that the topological phase shift vanishes as it should,

$$\phi_t^\pm = \oint dk'_y A_{0\pm} = \oint dk'_y \frac{k_x}{k_x^2 + (k'_y)^2} = 0 \quad (n = 0). \quad (13)$$

For the topological case, we consider the equi-energy contours

$$k_z^\pm(k_y) = \frac{\epsilon u \pm \sqrt{(u^2 - 1)(k_x^2 + k_y^2)^n + \epsilon^2}}{u^2 - 1}. \quad (14)$$

For $u > 1$, $k_z^\pm(k_y)$ are disjoint and we need to introduce an additional orbit segment that connects the two open ends of $k_z^\pm(k_y)$ at $k_z \rightarrow \pm\infty$. These connecting segment can be realized by an additional mass term

$\eta k_z^3 \sigma_z$ in the Hamiltonian, with an infinitesimal $\eta > 0$. The reconnection then occurs at large momenta k_z , with $|k_z| > (u-1)/\eta \rightarrow \infty$. In the expressions for A and M the additional mass term replaces $k_z \rightarrow k_z + \eta k_z^3$. On the connecting segment, A and M go to zero like η^2 , while the integration along the connecting segment gives a factor of order $1/\eta$. Hence the contribution of the connecting segment to ϕ_t vanishes and the integration reduces to the integration along the main contour $k_z^\pm(k_y)$. Inserting (11), (12), and (14) into (5) we obtain

$$\phi_t^\pm = \mp \int dk'_y \frac{(u+1)nk_x(k_x^2 + (k'_y)^2)^{n-1}}{2[k^{n\pm} \pm k_z^\pm][k_z^\pm \mp uk^\pm]}. \quad (15)$$

The integral depends on the topological charge n and the parameter θ encoding the details of the contour, defined as

$$\theta = \begin{cases} \text{atan}\left(\frac{k_x^n \sqrt{u^2-1}}{\epsilon}\right) & u > 1 \\ \text{atanh}\left(\frac{k_x^n \sqrt{1-u^2}}{\epsilon}\right) & u < 1. \end{cases} \quad (16)$$

For a type-II cone ($u > 1$) we use the substitution $\kappa = k'_y/k_x$ and obtain

$$\phi_t^\pm = \int_{-\infty}^{\infty} d\kappa \frac{n(\kappa^2+1)^{n-1}}{2\sqrt{(\kappa^2+1)^n + \cot^2 \theta}} \times \left(\sqrt{(\kappa^2+1)^n + \cot^2 \theta} \pm \cot \theta\right)^{-1}. \quad (17)$$

While ϕ_t^\pm are the topological phase shifts of the two orbits $k_z^\pm(k_y)$, the sum $\phi_t^+ + \phi_t^- \equiv \phi_t^{\text{br}}$ is the topological phase shift of the breakthrough orbit. The surprising result is now that for the breakthrough orbit the θ dependent part of the phase cancels. Using the substitution $z = (\kappa^2+1)^n$ the integral for ϕ_t^{br} simplifies to

$$\phi_t^{\text{br}} = \int_1^{\infty} dz \frac{1}{\sqrt{z^{\frac{2n+1}{n}} - z^2}} = n\pi, \quad (18)$$

which only depends on the value n of the topological charge.

For the separate orbits we find a closed-form solution for the case $n=1$ (see Appendix A for a detailed calculation),

$$\phi_t^\pm = \frac{\pi}{2}(1 \mp \text{sign}\theta) \pm \theta \quad (n=1). \quad (19)$$

The complete result for arbitrary n , obtained by evaluating (17) numerically, is shown in Fig. 2.

For a type-I cone ($u < 1$), k_z^\pm are two parts of a single closed contour, which topological phase is denoted ϕ_t . A closed-form solution for the integral (15) is found for $n=1$ (detailed calculation in Appendix B),

$$\phi_t = \pi \text{sign}\theta \quad (n=1), \quad (20)$$

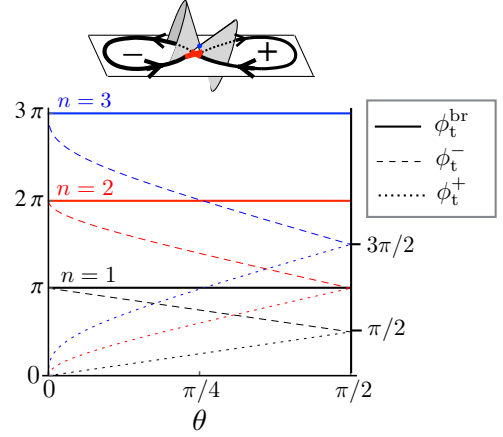


FIG. 2: Parameter dependence of the topological phase shift of orbits at a type-II Weyl node. The phase shifts of separate orbits k_z^\pm and k_z^- (without magnetic breakthrough) depend on the band parameter θ , while the phase shift of the figure-8 breakthrough orbit only depends on the topological charge n .

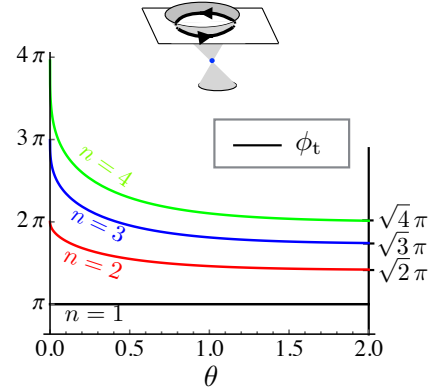


FIG. 3: Parameter dependence of the topological phase shift of orbits at a type-I Weyl node.

in agreement with Ref. [4]. For $n \geq 2$, we find in the limits $\theta \rightarrow 0^\pm$ and $\theta \rightarrow \pm\infty$,

$$\phi_t = \frac{\theta \rightarrow 0^\pm}{\rightarrow} n\pi \text{sign}\theta, \quad \phi_t = \frac{\theta \rightarrow \pm\infty}{\rightarrow} \sqrt{n}\pi \text{sign}\theta. \quad (21)$$

Figure 3 shows the full θ dependence of the phase.

Breakthrough phase shift—To calculate the additional phase shift of the breakthrough orbit at a type-II Weyl point, we follow a standard route [14] and calculate the scattering matrix that relates the exact wavefunction of the magnetic-breakdown region with the in- and outgoing semiclassical wavefunctions.

We start with the non-topological Hamiltonian H_0 . Introducing the magnetic field via Peierls substitution $k_z \mapsto k_z + il^{-2}\partial_{k_y}$, followed by a unitary transformation,

$$\tilde{H}_0 = e^{-il^2(k_z - \epsilon/u)k_y} H_0 e^{il^2(k_z - \epsilon/u)k_y}, \quad (22)$$

we arrive at

$$\tilde{H}_0 = k_x \sigma_x + k_y \sigma_y + u il^{-2} \partial_{k_y} \sigma_0 + \epsilon. \quad (23)$$

Rescaling the variables as $k = lk_y/\sqrt{u}$, $\delta_0 = lk_x/\sqrt{u}$, the Schrödinger equation $\tilde{H}_0\psi = \epsilon\psi$ reads

$$[\sigma_x\delta_0 + \sigma_y k + i\partial_k]\psi = 0. \quad (24)$$

The exact solution of (24) is known from the Landau-Zener problem [21]. To obtain the phase shift in comparison to the semiclassical solution of (24), the exact wavefunctions are matched with the incoming semiclassical wavefunctions at $k \ll -\delta_0$, denoted ψ_i^\pm , and outgoing ψ_f^\pm at $k \gg \delta_0$. From this standard procedure (recapitulated in Appendix C) we obtain the scattering matrix S that relates the final state in the basis (ψ_f^+, ψ_f^-) to the incoming state in the basis (ψ_i^+, ψ_i^-) ,

$$S = \begin{pmatrix} \sqrt{1-W} e^{i\alpha} & -i\sqrt{W} \\ -i\sqrt{W} & \sqrt{1-W} e^{-i\alpha} \end{pmatrix}, \quad (25)$$

where

$$W = e^{-\pi\delta_0^2}, \quad \alpha = \frac{\pi}{4} + \frac{\delta_0^2}{2} - \frac{\delta_0^2}{2} \ln \frac{\delta_0^2}{2} + \arg \Gamma\left(i\frac{\delta_0^2}{2}\right). \quad (26)$$

The breakthrough orbit dominates if $\delta_0 \ll 1$, $W \approx 1$, in which case each band transition in the breakthrough region contributes a phase jump of $\pi/2$ giving in total the phase shift $\phi_b = \pi$ for the breakthrough orbit.

For the topological case, we linearize the Hamiltonian H_n in k_y , leading to

$$H'_n = k_x^n \sigma_x + nk_x^{n-1} k_y \sigma_y + k_z \sigma_z + uk_z. \quad (27)$$

After Peierls substitution we apply the unitary transformation given by

$$\tilde{H}_n = e^{-i\ell^2[k_z - \epsilon/(u^2-1)]k_y} H'_n e^{i\ell^2[k_z - \epsilon/(u^2-1)]k_y}. \quad (28)$$

Rescaling and transforming the variables as

$$k = lk_y(u^2 - 1)^{-1/4} \sqrt{nk_x^{n-1}}, \quad (29a)$$

$$\delta_n = l \text{sign}(\epsilon) \frac{\sqrt{\epsilon^2 + (u^2 - 1)k_x^{2n}}}{(u^2 - 1)^{3/4} k_x^{(n-1)/2}}, \quad (29b)$$

we obtain the Schrödinger equation

$$\left[\delta_n \sqrt{u^2 - 1} \sin \theta \sigma_x + k \sqrt{u^2 - 1} \sigma_y + i\partial_k(u + \sigma_z) + \delta_n \cos \theta(1 + u\sigma_z) \right] \psi = 0. \quad (30)$$

Multiplying (30) from the left with $\mathcal{M} = \text{diag}[(u+1)^{-1}, (u-1)^{-1}]$ and applying a transformation given by

$$T = -i \begin{pmatrix} \frac{1-u}{\sqrt{u^2-1}} & \frac{u-1}{\sqrt{u^2-1}} \\ 1 & 1 \end{pmatrix} \sigma_z e^{-i\sigma_y \theta/2}, \quad (31)$$

we again arrive at the differential equation of the Landau-Zener form (24),

$$\hat{H}\hat{\psi}(k) = (\delta_n \sigma_x + k \sigma_y + i\partial_k)\hat{\psi}(k) = 0, \quad (32)$$

where $\hat{\psi}(k) = T^{-1}\psi(k)$ and $\hat{H} = T^{-1}\mathcal{M}\tilde{H}T$. The solution of (30) is thus given by the solution of the Landau-Zener problem multiplied from the left with the matrix T . Note that the θ phase brought into the full solution by the matrix T is the topological phase of the full solution induced by the non-trivial topology of the Hamiltonian.

The S matrix is obtained by matching $\psi(k)$ with the semiclassical solution of (30). Since H'_n is topologically equivalent to H_1 (note that the dynamical variables are k_y and k_z , while k_x is fixed), the topological phase shift of the semiclassical solution is given by (19), which cancels the θ phase of the full solution and the result is the same θ -independent scattering matrix (25), with δ_0 replaced by δ_n . In particular, the breakthrough phase shift $\phi_b = \pi$ also holds in the topological case.

Discussion—We have analyzed the shift of Landau levels associated with type-I and a type-II multi-Weyl fermions, focusing on the question how the shift depends on the topological charge. The most robust dependence is found in the case of magnetic breakthrough, where the topological charge of a type-II Weyl node is explored by a figure-8 orbit. Here the breakthrough contributes an offset 1/2 and the topological charge adds an extra contribution $n/2$. In contrast, without breakthrough or in case of a type-I Weyl node, the offset has in addition a characteristic dependence on band details.

Our calculations shed light on the recent numerical results for the offset of figure-8 breakthrough orbits of a thin-film Weyl semimetal [22] and a type-II Weyl semimetal [15], showing an offset of, respectively, 1/2 and 0. In case of the thin film, the Hamiltonian at the figure-8 crossing, given in the appendix of Ref. [22], is equivalent to the non-topological Hamiltonian H_0 , thus the only phase contributing is the breakthrough phase $\phi_b = \pi$, which explains the offset $\gamma = \phi_b/2\pi = 1/2$. In case of the type-II Weyl semimetal, the Hamiltonian is equivalent to H_1 , where the additional topological phase $\phi_t = \pi$ cancels the breakthrough phase, which explains the vanishing offset. This contradicts a previous interpretation that relates the vanishing offset of the latter to a vanishing Berry phase and neglects the contribution of the breakthrough phase [16].

Besides the relevance of our results for analyzing the oscillation phase shift of topological metals in general, a particular experimental observation is especially interesting with regard to the robust phase shift of breakthrough orbits. Recently magnetic breakthrough has been observed in quantum oscillations of the nodal-line semimetal ZrSiS [10], where strong indications of robust phase shifts of breakthrough orbits have been revealed, allowing to isolate the topological charge encircled by individual orbits.

Acknowledgements—The authors would like to thank Carlo Beenakker and Aris Alexandradinata for valuable discussions. This research was supported by the Netherlands Organization for Scientific Research (NWO/OCW) and an ERC Synergy Grant.

- [1] L. M. Roth, Phys. Rev. **145**, 434 (1966).
 [2] Y. Gao and Q. Niu, Proc. Natl. Acad. Sci. U. S. A. **114**, 7295 (2017).
 [3] G. P. Mikitik and Y. V. Sharlai, Phys. Rev. Lett. **82**, 2147 (1999).
 [4] J. Fuchs, F. Piéchon, M. Goerbig, and G. Montambaux, Eur. Phys. J. B **77**, 351 (2010).
 [5] A. Alexandradinata, C. Wang, W. Duan, and L. Glazman, Phys. Rev. X **8**, 011027 (2017).
 [6] Y. Zhang, Y.-W. Tan, H. L. Stormer, and P. Kim, Nature **438**, 201 (2005).
 [7] L. P. He, X. C. Hong, J. K. Dong, J. Pan, Z. Zhang, J. Zhang, and S. Y. Li, Phys. Rev. Lett. **113**, 246402 (2014).
 [8] X. Huang, L. Zhao, Y. Long, P. Wang, D. Chen, Z. Yang, H. Liang, M. Xue, H. Weng, Z. Fang, et al., Phys. Rev. X **5**, 031023 (2015).
 [9] J. Hu, Z. Tang, J. Liu, X. Liu, Y. Zhu, D. Graf, K. Myhro, S. Tran, C. N. Lau, J. Wei, et al., Phys. Rev. Lett. **117**, 016602 (2016).
 [10] S. Pezzini, M. R. van Delft, L. Schoop, B. Lotsch, A. Carrington, M. I. Katsnelson, N. E. Hussey, and S. Wiedmann, Nat. Phys. **14**, 178 (2017).
 [11] A. A. Burkov, Nat. Mater. **15**, 1145 (2016).
 [12] A. A. Soluyanov, D. Gresch, Z. Wang, Q. Wu, M. Troyer, X. Dai, and B. A. Bernevig, Nature **527**, 495 (2015).
 [13] M. H. Cohen and L. M. Falicov, Phys. Rev. Lett. **7**, 231 (1961).
 [14] M. I. Kaganov and A. A. Slutskin, Phys. Rep. **4**, 189 (1983).
 [15] T. E. O'Brien, M. Diez, and C. W. J. Beenakker, Phys. Rev. Lett. **116**, 236401 (2016).
 [16] A. Alexandradinata and L. I. Glazman, Phys. Rev. Lett. **119**, 256601 (2017).
 [17] C. Fang, M. J. Gilbert, X. Dai, and B. A. Bernevig, Phys. Rev. Lett. **108**, 266802 (2012).
 [18] J. B. Keller, Ann. Phys. (N. Y.) **4**, 180 (1958).
 [19] G. Panati, H. Spohn, and S. Teufel, Commun. Math. Phys. **242**, 547 (2003).
 [20] D. Xiao, M.-C. Chang, and Q. Niu, Rev. Mod. Phys. **82**, 1959 (2010).
 [21] L. D. Landau and E. M. Lifshitz, *Course of Theoretical Physics* (Elsevier, Oxford, 1977).
 [22] N. Bovenzi, M. Breitenkreiz, T. E. O'Brien, J. Tworzydło, and C. W. J. Beenakker, New J. Phys. **20**, 023023 (2018).
 [23] A. Alexandradinata and L. I. Glazman, arXiv: 1710.04215.

Appendix A: Topological phase for $u > 1$

While the sum of the phases ϕ_t^\pm has been calculated in the main text, to obtain each of the phases separately we now focus on the difference. From (17) we find

$$\phi_t^- - \phi_t^+ = \int_{-\infty}^{\infty} d\kappa \frac{n \cot \theta}{(\kappa^2 + 1) \sqrt{(\kappa^2 + 1)^n + \cot^2 \theta}}. \quad (\text{A1})$$

Using the series expansion

$$\frac{1}{\sqrt{1+q}} = \sum_{m=0}^{\infty} \binom{m - \frac{1}{2}}{m} (-q)^m \quad (\text{A2})$$

and the integral

$$\int_{-\infty}^{\infty} d\kappa \frac{1}{(\kappa^2 + 1)^\alpha} = \frac{\sqrt{\pi} \Gamma(\alpha - \frac{1}{2})}{\Gamma(\alpha)}, \quad (\text{A3})$$

Eq. (A1) can be written as

$$\begin{aligned} \phi_t^- - \phi_t^+ &= n \cot \theta \sum_{m=0}^{\infty} (-1)^m \binom{m - \frac{1}{2}}{m} \\ &\times \frac{\sqrt{\pi} \Gamma(nm + \frac{n+1}{2})}{\Gamma(nm + \frac{n+2}{2})} (\cot \theta)^{2m}. \end{aligned} \quad (\text{A4})$$

For $n = 1$ the series is the expansion of $2 \arctan(\cot \theta) / \cot \theta$, which gives

$$\phi_t^- - \phi_t^+ = \text{sign}(\theta) \pi - 2\theta. \quad (\text{A5})$$

Together with (18), $\phi_t^- + \phi_t^+ = n\pi$, this leads to

$$\phi_t^\pm = \frac{\pi}{2} (1 \mp \text{sign} \theta) \pm \theta. \quad (\text{A6})$$

Appendix B: Topological phase for $u < 1$

For $u < 1$, k_z^\pm are two parts of a single closed contour. The phase ϕ_t of the contour is thus given by the difference $\phi_t = \phi_t^+ - \phi_t^-$, where, using (15), (16), and the substitution $\kappa = k'_y/k_x$, ϕ_t^\pm are given by

$$\phi_t^\pm = - \int_{-\kappa_0}^{\kappa_0} d\kappa \frac{n(\kappa^2 + 1)^{n-1}}{2\sqrt{\coth^2 \theta - (\kappa^2 + 1)^n}} \quad (\text{B1})$$

$$\times \left(\sqrt{\coth^2 \theta - (\kappa^2 + 1)^n} \pm \coth \theta \right)^{-1}, \quad (\text{B2})$$

where $\kappa_0 = \sqrt{(\coth \theta)^{2/n} - 1}$. The difference reduces to

$$\phi_t = \int_{-\kappa_0}^{\kappa_0} d\kappa \frac{n \coth \theta}{(\kappa^2 + 1) \sqrt{\coth^2 \theta - (\kappa^2 + 1)^n}} \quad (\text{B3})$$

and, after the substitution $z = (\kappa^2 + 1)^n$, can be rewritten as

$$\phi_t = \int_1^{\coth^2 \theta} dz \frac{\coth \theta}{z \sqrt{\coth^2 \theta - z} z^{1/n} - 1}. \quad (\text{B4})$$

A closed-form solution is found for $n = 1$,

$$\phi_t = \pi \text{sign} \theta. \quad (\text{B5})$$

For a general n we find in the limits $\theta \rightarrow 0^\pm$

$$\phi_t \xrightarrow{\theta \rightarrow 0^\pm} n \pi \text{sign} \theta \quad (\text{B6})$$

and $\theta \rightarrow \pm\infty$

$$\phi_t \xrightarrow{\theta \rightarrow \pm\infty} \sqrt{n} \pi \text{sign} \theta. \quad (\text{B7})$$

Appendix C: Scattering matrix for magnetic breakdown

a. Non-topological Hamiltonian

To obtain the full solution in the magnetic-breakthrough region, we solve the differential equation

$$[\sigma_x \delta + \sigma_y k + i \partial_k] \psi = 0. \quad (\text{C1})$$

Multiplying from the left with $U = \exp(-i\sigma_x \pi/4)$ and inserting the ansatz $\psi = U^\dagger(\eta, \xi)^T$ we obtain

$$(k^2 + \partial_k^2 - i + \delta^2) \eta = 0, \quad (\text{C2})$$

$$\xi = -\delta^{-1}(k + i \partial_k) \eta. \quad (\text{C3})$$

Equation (C2) can be transformed to Weber's equation for the parabolic cylinder function,

$$\eta'' - \left(\frac{1}{4}z^2 + a\right)\eta = 0, \quad (\text{C4})$$

where

$$z = \sqrt{2}e^{i\pi/4}k, \quad a = \frac{1}{2} + i\gamma, \quad \gamma = \frac{1}{2}\delta^2. \quad (\text{C5})$$

The two solutions read

$$\eta_a = e^{-z^2/4} {}_1F_1\left(\frac{1}{2}a + \frac{1}{4}; \frac{1}{2}; \frac{1}{2}z^2\right), \quad (\text{C6a})$$

$$\eta_b = z e^{-z^2/4} {}_1F_1\left(\frac{1}{2}a + \frac{3}{4}; \frac{3}{2}; \frac{1}{2}z^2\right), \quad (\text{C6b})$$

where ${}_1F_1()$ is the confluent hypergeometric function. Its general asymptotic form for a large last argument reads

$${}_1F_1(\alpha, \beta, ik^2) \xrightarrow{k \rightarrow \infty} \Gamma(\beta) \left(\frac{1}{\Gamma(\alpha)} e^{ik^2} (ik^2)^{\alpha-\beta} + \frac{1}{\Gamma(\beta-\alpha)} (-ik^2)^{-\alpha} \right). \quad (\text{C7})$$

From this we obtain the asymptotic form of the two solutions (C6),

$$\eta_a = \frac{\Gamma(\frac{1}{2})}{\Gamma(\gamma\frac{i}{2} + \frac{1}{2})} e^{ik^2/2 + i\gamma \ln |k| - \pi\gamma/4}, \quad (\text{C8a})$$

$$\eta_b = \text{sign}(k) \frac{\sqrt{2}\Gamma(\frac{3}{2})}{\Gamma(\gamma\frac{i}{2} + 1)} e^{ik^2/2 + i\gamma \ln |k| - \pi\gamma/4}. \quad (\text{C8b})$$

Inserting into (C3), we obtain the two corresponding expressions for ξ ,

$$\xi_a = -\text{sign}(k) \frac{\sqrt{2\pi/\gamma}}{\Gamma(-\gamma\frac{i}{2})} e^{-ik^2/2 - i\gamma \ln |k| + i\pi/4 - \pi\gamma/4}, \quad (\text{C9a})$$

$$\xi_b = -\frac{\sqrt{\pi/\gamma}}{\Gamma(\frac{1}{2} - \gamma\frac{i}{2})} e^{-ik^2/2 - i\gamma \ln |k| + i3\pi/4 - \pi\gamma/4}. \quad (\text{C9b})$$

Altogether, an arbitrary solution of (C1) at $|k| \gg \delta$ is thus the linear combination

$$\psi(k) = e^{i\sigma_x \pi/4} \Psi(k) \mathbf{a}, \quad \Psi(k) = \begin{pmatrix} \eta_a & \eta_b \\ \xi_a & \xi_b \end{pmatrix}, \quad \mathbf{a} = \begin{pmatrix} a_1 \\ a_2 \end{pmatrix}, \quad (\text{C10})$$

where a_1, a_2 are arbitrary coefficients.

The approximate semiclassical solution of (C1) reads [14, 23]

$$\psi_s(k) = \chi(k) e^{-i \int_0^k dk' k_z(k') + \phi_t(k)}, \quad (\text{C11})$$

where $\chi(k)$ and $k_z(k)$ are determined by

$$[\sigma_x \delta + \sigma_y k + k_z^\pm(k)] \chi_\pm(k) = 0, \quad (\text{C12})$$

$$k_z^\pm(k) = \pm \sqrt{k^2 + \delta^2} \quad (\text{C13})$$

and $\phi_t(k)$ is the topological phase shift accumulated on the orbit section between $k_y = 0$ and $k_y = k$,

$$\begin{aligned} \phi_t(k) &= i \int_0^k dk'_y \chi_\pm^\dagger(k) \partial_k \chi_\pm(k) = \int_0^k dk' \frac{\delta}{2(\delta^2 + (k')^2)} \\ &= \arctan(k/\delta)/2. \end{aligned} \quad (\text{C14})$$

The first term in the exponent of the semiclassical wavefunction can be written as

$$\int_0^k dk' k_z^\pm(k') = \pm \text{sign}(k) f(k) + \mathcal{O}(\delta_0^2/k^2), \quad (\text{C15a})$$

$$f(k) = \frac{1}{2} [k^2 + \delta_0^2 (\ln |2k/\delta_0| + 1/2)]. \quad (\text{C15b})$$

The basis for the scattering matrix is formed by the semiclassical wavefunctions at $k \ll -\delta$ as incoming states ψ_i and at $k \gg \delta$ as outgoing states ψ_f . To leading order in δ/k we obtain

$$\psi_i^\pm = e^{\pm i f(k)} \frac{1}{\sqrt{2}} \begin{pmatrix} \mp e^{i\pi/4} \\ e^{-i\pi/4} \end{pmatrix}, \quad (\text{C16})$$

$$\psi_f^\pm = e^{\mp i f(k)} \frac{1}{\sqrt{2}} \begin{pmatrix} \mp e^{-i\pi/4} \\ e^{i\pi/4} \end{pmatrix} \quad (\text{C17})$$

and combine the scattering states into matrices,

$$\Psi_i(k) = (\psi_i^+, \psi_i^-), \quad \Psi_f(k) = (\psi_f^+, \psi_f^-). \quad (\text{C18})$$

We choose the coefficients of the full solution, \mathbf{a} , such that at $k_y \ll -\delta$ the full solution coincides with the incoming state, $\Psi_i \mathbf{c}_i$, where according to (C18), $\mathbf{c}_i = (1, 0)$ corresponds to incoming state ψ_i^+ and $\mathbf{c}_i = (0, 1)$ corresponds to incoming state ψ_i^- . At $k \gg \delta$ the phase and amplitude of the final states, combined in \mathbf{c}_f , is then determined by matching $\psi(k)$ with $\Psi_f \mathbf{c}_f$. Altogether, the matching conditions read

$$\Psi_i(k \ll -\delta) \mathbf{c}_i = \Psi(k \ll -\delta) \mathbf{a}, \quad (\text{C19})$$

$$\Psi(k \gg \delta) \mathbf{a} = \Psi_f(k \gg \delta) \mathbf{c}_f. \quad (\text{C20})$$

Eliminating \mathbf{a} we obtain the expression for the scattering matrix S

$$\mathbf{c}_f = \underbrace{\Psi_f(k)^{-1} \Psi(k) \Psi^{-1}(-k) \Psi_i(-k)}_{\equiv S} \mathbf{c}_i, \quad k/\delta \rightarrow +\infty. \quad (\text{C21})$$

Inserting the expressions $\Psi_f(k)$, $\Psi_i(k)$, and $\Psi(k)$ given above, we obtain the scattering matrix (25) given in the main text.

b. *Topological Hamiltonian*

We consider the Schrödinger equation

$$\left[\delta_n \sqrt{u^2 - 1} \sin \theta \sigma_x + k \sqrt{u^2 - 1} \sigma_y + i \partial_k (u + \sigma_z) + \delta_n \cos \theta (1 + u \sigma_z) \right] \psi = 0. \quad (\text{C22})$$

The semiclassical solution reads

$$\psi_s(k) = \chi(k) e^{-i \int_0^k dk' k_z(k') + \phi_t(k)}, \quad (\text{C23})$$

where $\chi(k)$ and $k_z(k)$ are given by

$$\left[\delta_n \sqrt{u^2 - 1} \sin \theta \sigma_x + k \sqrt{u^2 - 1} \sigma_y + k_z^\pm(k) (u + \sigma_z) + \delta_n \cos \theta (1 + u \sigma_z) \right] \chi_\pm(k) = 0, \quad (\text{C24})$$

$$k_z^\pm(k) = \pm \sqrt{k^2 + \delta_n^2}. \quad (\text{C25})$$

The phase $\int_0^k dk' k_z^\pm(k')$ is in analogy to the non-topological case given by (C15) (with δ_0 replaced by δ_n). The topological phase shift is most easily obtained by considering the original Schrödinger equation

$$H'_n \psi = \epsilon \psi, \quad (\text{C26})$$

$$H'_n = k_x^n \sigma_x + n k_x^{n-1} k_y \sigma_y + k_z \sigma_z + u k_z, \quad (\text{C27})$$

which is related to (C22) by a k_z shift introduced in (28) in the main text, which leaves the phase shift accumulated between $k = 0$ and $k = \pm\infty$ invariant. The Hamiltonian is of the form of H_1 . The topological phase shift thus calculates in analogy to the phase $\phi_t^{1\pm}$ of the main text. Since by symmetry the phase shift from $k = 0$ to

$k = \pm\infty$ is half the phase shift from $k = -\infty$ to $k = \infty$, we can use Eq. (19) to obtain

$$\phi_t^{n\pm}(k = \infty) = \frac{\pi}{4} (1 \mp \text{sign} \theta) \pm \frac{\theta}{2}, \quad (\text{C28})$$

which is sufficient for the in- and outgoing states at $k = \pm\infty$. Together with the spinors from (C24) the scattering states read

$$\psi_i^\pm = e^{\pm i f(k) - i \frac{\pi}{4} (1 \mp \text{sign} \theta) \mp i \theta / 2} \begin{pmatrix} \mp i \sqrt{\frac{u-1}{2u}} \\ \sqrt{\frac{u+1}{2u}} \end{pmatrix}, \quad (\text{C29a})$$

$$\psi_f^\pm = e^{\mp i f(k) + i \frac{\pi}{4} (1 \mp \text{sign} \theta) \pm i \theta / 2} \begin{pmatrix} \pm i \sqrt{\frac{u-1}{2u}} \\ \sqrt{\frac{u+1}{2u}} \end{pmatrix}. \quad (\text{C29b})$$

To find the full solution $\psi(k)$ we multiply (C22) from the left with $\mathcal{M} = \text{diag}[(u+1)^{-1}, (u-1)^{-1}]$ and apply a transformation given by

$$T = -i \begin{pmatrix} \frac{1-u}{\sqrt{u^2-1}} & \frac{u-1}{\sqrt{u^2-1}} \\ 1 & 1 \end{pmatrix} \sigma_z e^{-i \sigma_y \theta / 2}, \quad (\text{C30})$$

which leads to the differential equation of the Landau-Zener form (C1),

$$\hat{H} \hat{\psi}(k) = (i \partial_k \sigma_0 + \delta_n \sigma_x + k \sigma_y) \hat{\psi}(k) = 0, \quad (\text{C31})$$

where $\hat{\psi}(k) = T^{-1} \psi(k)$ and $\hat{H} = T^{-1} \mathcal{M} \tilde{H} T$. As in the non-topological case, we obtain the S matrix by matching the full solution with the scattering states, $T^{-1} \psi_{i/f}^\pm$, which leads to the scattering matrix (25) with δ_0 replaced by δ_n .